Critical behavior of pure and site-random two-dimensional antiferromagnets

R. J. Birgeneau
Department of Physics, Massachusetts Institute of Technology, Cambridge, Massachusetts 02139 and Bell Laboratories, Murray Hill, New Jersey 07974*

J. Als-Nielsen
Department of Physics, Massachusetts Institute of Technology, Cambridge, Massachusetts 02139 and Research Establishment Risø, Roskilde, DK-4000 Denmark*

G. Shirane
Brookhaven National Laboratory,† Upton, New York 11973

(Received 17 February 1977)

Quasielastic neutron scattering studies of the static critical behavior in the two-dimensional antiferromagnets K_2NiF_4, K_2MnF_4, and $Rb_2Mn_{0.5}Ni_{0.5}F_4$ are reported. For $T < 0.95T_N$ the diffuse scattering arises principally from the noncritical transverse susceptibility $\chi^{\perp}(\vec{Q})$. In all three materials $\chi^{\perp}(\vec{Q})$ is found to be only weakly temperature dependent for $T < T_N$ with a half width, $\kappa^{\perp}$, consistent with spin-wave theory. For $|1 - T/T_N| < 0.05$ the overall scattering is dominated by the critical Ising component $\chi^{\parallel}(\vec{Q})$. The total scattering is proportional to $\chi^{\parallel}(\vec{Q}) + \chi^{\perp}(\vec{Q})$ so that, with an appropriate correction for $\chi^{\perp}(\vec{Q})$, the detailed critical behavior for $\chi^{\parallel}(\vec{Q})$ may be determined. For the reduced temperature range $0.008 < T/T_N - 1 < 0.15$ one finds in all three materials $\nu = 0.9 \pm 0.1$, $\gamma = 1.6 \pm 0.15$, and from the scaling relation $\gamma = \nu(2 - \eta)$, $\eta = 0.2 \pm 0.05$. For $T < T_N$ one finds $\beta = 0.15 \pm 0.015$ in the three systems. Finally, in K_2NiF_4 for $T < T_N$, $\chi^{\parallel}(0)$, and $\kappa^{\parallel}$ are consistent with two-dimensional Ising behavior with exponents $\gamma' = 1.75$, $\nu' = 1$; further $\chi^{\parallel}(+|\epsilon|) \simeq (50 \pm 10)\chi^{\parallel}(-|\epsilon|)$ compared with the Ising asymmetry factor of 37. These results thence demonstrate that the site-random and pure systems have identical critical behavior in agreement with current theory. Further, the critical behavior is close to that of the two-dimensional Ising model, although there are small differences assumedly due to the fact that the experiments do not probe the true asymptotic region. Finally a number of inconsistencies in earlier experiments are resolved.

I. INTRODUCTION

In the past decade a vast range of experiments and theoretical calculations have been performed on the planar antiferromagnet K_2NiF_4 and its isomorphs.[1] The principal reason for this extensive interest is that the K_2NiF_4 compounds exhibit almost ideal two-dimensional (2D) cooperative behavior.[2] The simplest systems are K_2CoF_4 and Rb_2CoF_4; recent experiments show that these compounds exhibit accurate 2D Ising critical and precritical behavior.[3] Hence they provide physical realizations of what, at one time seemed to be an abstract, albeit most important, mathematical statistical mechanical model.[4] The $Ni^{++}(S=1)$ and $Mn^{++}(S=\frac{5}{2})$ isomorphs correspond closely to nearest-neighbor (nn) square-lattice Heisenberg antiferromagnets.[1,2] It was hoped originally that experiments on these antiferromagnets would serve to elucidate the phase transition behavior of 2D systems with a continuous symmetry.[5] It is now clear however, that in all cases studied to date "real Hamiltonian" as opposed to "idealized Hamiltonian" effects play an important role in the critical region.[6-8] Hence although these near-isotropic systems are still of considerable intrinsic interest, they do not cast light on the 2D continuous symmetry phase transition problems.

As noted above, the compounds K_2NiF_4 and K_2MnF_4 have been extensively investigated.[1] In both cases the principal term in the spin Hamiltonian is the nn isotropic exchange. There is in addition a small Ising anisotropy arising from crystal-field effects in K_2NiF_4 and from the magnetic dipole-dipole interaction in K_2MnF_4. The static and dynamic properties of these systems at low temperatures may be understood in detail using conventional spin-wave theory. This includes the temperature-dependent spin-wave dispersion relations, the zero-point spin deviation, the sublattice magnetization, and the transverse and longitudinal bulk susceptibilities.[1,2,9] Similarly at high temperatures, that is, $T > 1.5T_N$, the macroscopic properties are well understood using conventional theory.

Our current picture of the detailed behavior in the critical region is, however, rather less satisfactory. Based on universality considerations one would expect a crossover from 2D Heisenberg behavior far from T_N to 2D Ising behavior in the critical region.[10] This expectation is indeed fulfilled in the order-parameter measurements below T_N; here one finds $\beta \simeq 0.14$ to 0.15 for the two materials in reasonable agreement with the 2D Ising

value[4] of 0.125. The situation above T_N is, however, more complicated. Birgeneau *et al.*[6,7] find that only $\chi''(0)$, the longitudinal component of the staggered susceptibility, diverges at T_N in K_2NiF_4 in agreement with one's expectations based on the Ising picture. However, from their quasielastic neutron critical scattering spectra they deduce the exponents $\gamma \sim 1$ for the staggered susceptibility and $\nu \simeq 0.6$ for the correlation length. In a similar experiment in K_2MnF_4, Ikeda and Hirakawa[8] also find mean-field-like exponents above T_c. The 2D Ising values[4] are $\gamma = 1.75$, $\nu = 1$ so that the above values represent a major discrepancy.

As discussed extensively in Ref. 7, these results are most unusual, and indeed, since 1971 no satisfactory explanation has been offered for them. Because of the current interest in the critical behavior of random systems[11] we have carried out an extensive study of the site-random antiferromagnet $Rb_2Mn_{0.5}Ni_{0.5}F_4$. This in turn has led us to reexamine the critical behavior of the pure systems. In this paper therefore we report a complete study of the static critical behavior of both the pure 2D antiferromagnets K_2NiF_4 and K_2MnF_4 and the random system $Rb_2Mn_{0.5}Ni_{0.5}F_4$. This involves new experiments below T_N in K_2NiF_4 and a complete set of experiments above and below T_N in K_2MnF_4 and $Rb_2Mn_{0.5}Ni_{0.5}F_4$. All three systems have then been analyzed together using identical techniques. Some of the theoretical uncertainties existent in 1971 have since been clarified so that our analysis has been guided by more recent theoretical developments. We note especially the work on $\chi''(\vec{q})$ for the 2D Ising model by Tracy and McCoy[12] and the computer simulations on the 2D anisotropic Heisenberg system by Binder and Landau.[13]

Our new experiments and analysis yield 2D Ising-like exponents for all three systems. Thus we believe that all aspects of these materials are now consistent with the most simple physical model. The essential difficulty in the previous analyses was in the treatment of the noncritical transverse susceptibility $\chi^{\perp}(\vec{q})$. Birgeneau *et al.*,[7] using quasielastic data above T_c alone, argued that in their experiment $\chi^{\perp}(\vec{q})$ could be absorbed into the background very near T_c. Our new data below T_c in K_2NiF_4 show that this approximation is definitely incorrect and that rather $\chi^{\perp}(\vec{q})$ must be included explicitly in the analysis. Ikeda and Hirakawa[8] in their experiments on K_2MnF_4, recognized the importance of $\chi^{\perp}(\vec{q})$ and apparently included some correction for it although their report is too brief for us to be able to assess any possible caveats. In any case, in our high-resolution experiments in K_2MnF_4 we find that when $\chi^{\perp}(\vec{Q})$ is included explicitly one obtains Ising-like exponents in K_2MnF_4 for $\chi''(\vec{q})$ in explicit disagreement with the Ikeda-Hirakawa results. Our final results as well as the method of analysis we have developed, both of which were deduced completely independently of the computer experiments by Binder and Landau,[13] are entirely consistent with this latter work. A brief note on the random system results has been published previously.[14]

The format of this paper is as follows. In Sec. II we give preliminary details including the spin Hamiltonian, magnetic structure, etc. In Sec. III the order-parameter measurements for $Rb_2Mn_{0.5}Ni_{0.5}F_4$ are reported. Section IV describes the quasielastic critical scattering measurements, analysis and results in all three systems. A general discussion including the connection between this work and related experiments together with concluding remarks are given in Sec. V.

II. PRELIMINARY DETAILS

A. Samples

The K_2NiF_4 and K_2MnF_4 crystals were the same as reported on earlier.[2,7] The site-random crystal $Rb_2Mn_{0.5}Ni_{0.5}F_4$ came from the same boule as the crystal we used for investigating the spin dynamics and the reader is referred to the dynamics paper[15] for further details concerning the growth techniques, assessment of randomness, etc. The present crystal had a considerably sharper transition temperature than that used in Ref. 15. Its dimensions were about $1 \times 6 \times 8$ mm. Ideally, we would have preferred a sample with the alkali atom K^+ rather than Rb^+. However, it turned out that very good quality crystals of $Rb_2Mn_{0.5}Ni_{0.5}F_4$ were available, whereas the mixed K^+ compounds were less satisfactory. From previous studies[1] it is known that the potassium and rubidium isomorphs have virtually identical magnetic properties so that intercomparison of the two, pure and random, is valid.

B. Hamiltonian and magnetic structure

The crystal structure is shown in the right part of Fig. 1. Values of the lattice constants are given in Table I. The magnetic ions are situated on a square lattice in planes perpendicular to the c axis. These planes are separated by *two* intervening planes of nonmagnetic ions so the superexchange coupling between spins of magnetic ions in different planes is extremely weak. Within the plane the spins are coupled antiferromagnetically by a nearest-neighbor superexchange coupling and they are also subject to a relatively small Ising anisotropy field arising from a combination of dipolar spin-spin interaction (for the Mn^{++} ions) and single-ion

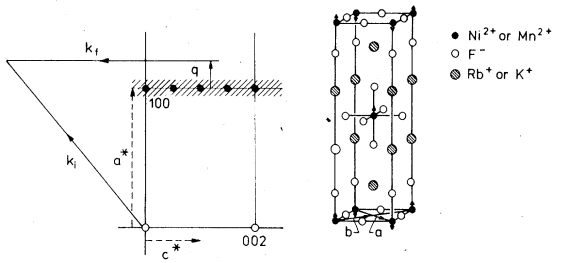

FIG. 1. Chemical unit cell and magnetic structure of the K_2NiF_4 type and the corresponding reciprocal-lattice plane (h,o,l). The critical scattering depends only on q, i.e., the distance from the $h=1$ line in reciprocal space. When $\vec{k}_f$ is parallel to c^*, the quasielastic approximation becomes exact.

crystal-field anisotropy (for the Ni^{++} ions). The spin Hamiltonian may to a good approximation be written

$$\mathcal{H}=\sum_{\substack{i>j\\ i,j \text{ nearest neighbors}}} J_{ij}\vec{S}_i\cdot\vec{S}_j+\sum_i g_i\mu_B H_i^A S_i^z, \tag{1}$$

where the anisotropy field H_i^A represents the combined effects of the dipolar and single-ion anisotropies. Values of J_{ij} for Mn-Mn, Ni-Ni, and Mn-Ni interactions are given in Table I as well as the anisotropy field expressed relative to the exchange field by

$$h_i^A=g\mu_B H_i^A\Big/\sum_j J_{ij}S_j. \tag{2}$$

We now consider the various magnetic structures and the corresponding scattering in reciprocal space. The simplest structure is the so-called K_2NiF_4 magnetic structure illustrated in Fig. 1. Here we choose as basis vectors for the magnetic cell the face diagonals $\vec{a},\vec{b}$ (see Fig. 1) while the tetragonal axis $\vec{c}$ coincides with the nuclear c axis. The extinction rules for this orthorhombic magnetic cell are that magnetic Bragg peaks will occur for h odd, k,l even and h even, k,l odd. Thus in the (hol) plane of reciprocal space magnetic Bragg peaks will appear when h is odd and $l=0,2,4$, etc. In addition, the central spin may be reversed in some domains of the crystals, reflecting the fact that the coupling between the planes is weak; in that case the h and k axes are interchanged so that the Bragg peaks occur when $l=1,3,\ldots$. Finally, in the mixed crystal, there are domains where the direction of the spins in the top plane is reversed (the Ca_2MnO_4 structure[16]) implying Bragg peaks occurring when $l=\frac{1}{2},\frac{3}{2},\frac{5}{2},\ldots$. We note also that if the spin directions from plane to plane are in fact uncorrelated but exhibit long-range order *within* each plane, the corresponding Bragg scattering occurs not in Bragg *points* but in Bragg *rods* with $h=1,3,\ldots$.

We now discuss the general temperature behavior. If, beginning at high temperatures, the temperature is lowered towards T_N, the correlations within each plane becomes longer and longer and ultimately there is a crossover from two-dimensional to three-dimensional behavior due to the small but finite interaction between the next-nearest-neighbor planes. The different types of three-dimensional magnetic structures described above are formed in different domains and the Bragg rod never occurs but rather precipitously condenses into Bragg points with $l=0,\frac{1}{2},1,\frac{3}{2}$, etc. In fact, in all systems investigated to date including those discussed here, the 3D critical region seems to be smaller than the intrinsic smearing of T_N due to strains, chemical gradients, etc. We should emphasize that *a priori* it is by no means obvious that the 3D critical region should be unobservably small. As is evident from the antiferromagnetic structure the coupling between adjacent planes only vanishes in a mean-field sense.[17] One might have expected however that fluctuation effects would produce an effective coupling between the nn planes thence leading to 3D correlations. These assumedly would be especially important in the site-random crystal. In fact, however, such effects must be extremely small. It is, of course, always possible that such a mechanism is operative but that the exchange interaction between the adjacent planes is simply too weak for the effects to be important.

TABLE I. Lattice constant, nearest-neighbor exchange, Néel temperature, and relative anisotropy field.

Compound	a[a] (Å)	J_{Mn-Mn} (K)	J_{Mn-Ni} (K)	J_{Ni-Ni} (K)	S	T_N (K)	h_A
K_2NiF_4	3.994	•••	•••	104	1	97.23	0.0021
K_2MnF_4	4.160	8.4	•••	•••	$\frac{5}{2}$	42.17	0.0038
$Rb_2Mn_{0.5}Ni_{0.5}F_4$	4.121	7.4	25.7	89	1, $\frac{5}{2}$	68.72	0.0071[b]

[a] Value at T_N.

[b] Value corresponding to the average of the fields on a Mn and a Ni site surrounded by 2 Mn and 2 Ni ions.

III. ORDER PARAMETER IN $Rb_2Mn_{0.5}Ni_{0.5}F_4$

We now discuss our measurements of the order parameter in $Rb_2Mn_{0.5}Ni_{0.5}F_4$. The order parameter, that is the staggered magnetization, is determined by the intensity of magnetic Bragg scattering. If the Bragg scattering is sufficiently weak that the neutron beam is not attenuated appreciably in traversing the crystal, the intensity of the Bragg scattering is simply proportional to the order parameter squared.[18] The degree of extinction may be determined by comparing different magnetic Bragg reflections. Measurements of this kind have been reported earlier[6] for K_2NiF_4 and for[2] K_2MnF_4 and results for the parameters in the power law

$$M(T)/M(0) = B(1 - T/T_N)^{\beta} \tag{3}$$

are given in Table II. Here we shall report on data for the mixed crystal $Rb_2Mn_{0.5}Ni_{0.5}F_4$. As discussed by Als-Nielsen *et al.*,[15] in this material there are domains where the nn planes are ferromagnetically aligned and others where the nn planes are oriented antiferromagnetically so in the $(h\,o\,l)$ plane magnetic Bragg peaks occur whenever h is odd and l is an integer or a half integer. The domains have identical critical temperatures and exhibit the same temperature dependence of the order parameter. As an example, the $(1\,0\,\frac{1}{2})$ Bragg intensity versus temperature is shown in Fig. 2. It is clear that the sample has a smeared Néel temperature. This rounding does not appear to be an intrinsic feature of the site-random system as it varies in magnitude from sample to sample. We have found empirically that the smearing is approximately proportional to the dimension of the sample along its c axis and consequently we suggest that the rounding is caused principally by a macroscopic concentration gradient along the c axis in the crystalline boule from which all samples were cut rather than by microscopic concentration fluctuations. In order to describe the smearing more quantitatively we assume that the Néel temperatures of the sample have a Gaussian distribution[15] with standard deviation σ. A least-squares fit of

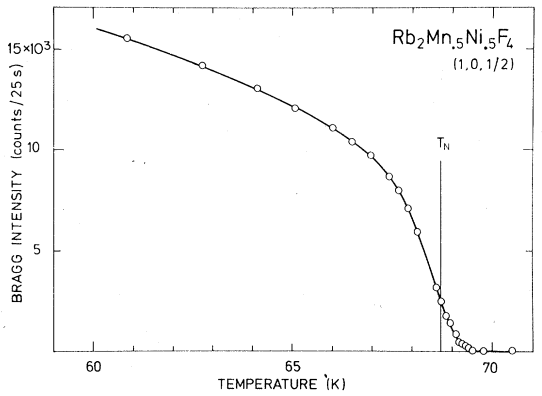

FIG. 2. Squared long-range order vs temperature in the site-random alloy. The smearing of T_N is probably due to a macroscopic concentration gradient through the crystal.

the data to

$$\frac{I_B(T)}{I_B(0)} = B^2 \int \left(\frac{T_N - T}{T_N}\right)^{2\beta} \exp\left(\frac{-(T_N - \langle T_N\rangle)^2}{2\sigma^2}\right) dT_N \tag{4}$$

yields

$$B = 1.015, \quad \beta = 0.163 \pm 0.004, \qquad \langle T_N\rangle = 68.72 \pm 0.01 \text{ K}, \quad \sigma = 0.42 \pm 0.01 \text{ K}. \tag{5}$$

The smearing as expressed by σ is about a factor of 5 less than that in a larger crystal reported on earlier. We note also that the Néel temperature of this sample differs by 5 K from that appropriate to the large sample used in the spin-dynamics studies.[15] This corresponds to a change in concentration of at least 5% across the boule. This in turn is consistent with our suggestion above that the observed smearing of $\sigma = 0.42$ K arises from macroscopic chemical gradients.

It is possible with the present crystal to study the static correlation function in the critical region.[11] As we shall see the limitation of our experimental data for the correlation function is *not* set by the smearing of T_N but rather by the in-

TABLE II. Critical exponents and amplitudes. Note that the reduced temperatures $t_c \equiv |T/T_N - 1|$ and $t \equiv |1 - T_N/T|$ have different limiting values for $T \to 0$ or $T \to \infty$.

Compound	$M/M_0 = Bt_c^{\beta}$ β	B	$a\kappa = F_c^{\nu}$ ν	F	$\frac{\chi(q=0)}{\chi^0} \propto t^{-\gamma}$ γ	$\chi T\kappa \propto t_c^{\nu\eta} t^{\nu\eta}$ $\nu\eta$	$\nu\eta$
K_2NiF_4	0.14	1.0	0.9	0.25	1.65	0.17	0.22
K_2MnF_4	0.15	1.0	0.95	0.47	1.65	0.16	0.20
$Rb_2Mn_{0.5}Ni_{0.5}F_4$	0.16	1.0	0.9	0.56	1.6	0.20	0.27
	±0.01	±0.03	±0.1		±0.15		

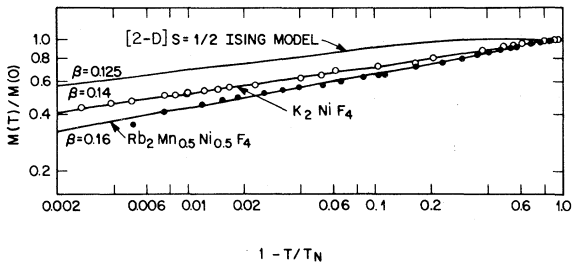

FIG. 3. Comparison of the long-range order vs temperature in the site-random alloy, the pure material K_2NiF_4 and the 2D Ising model.

strumental wavevector resolution. The data for $M(T)/M(0)$ vs $(1-T/T_N)$ is shown in a double log plot in Fig. 3 for the site-random system as well as for the pure system K_2NiF_4. The critical exponent of the order parameter for the pure and random systems are very similar and not far from the 2D Ising model value. We emphasize that there is no *a priori* reason to assume a Gaussian distribution of Néel temperatures—Eq. (4) merely serves as a simple technique for including the effects of smearing.

IV. CRITICAL FLUCTUATIONS

A. Neutron scattering

In the left-hand part of Fig. 1 we show the scattering diagram corresponding to the process where neutrons incident with wave vector $\vec{k}_i$ are scattered to wave vector $\vec{k}_f$. The cross section[18] depends on the momentum transfer $\hbar\vec{Q}=\hbar(\vec{k}_i-\vec{k}_f)$ and the energy transfer $\hbar\omega=(\hbar^2/2m)(k_i^2-k_f^2)$:

$$\sigma(\vec{k}_i\to\vec{k}_f)\propto\sum_{\alpha\beta}\left(\delta_{\alpha\beta}-\frac{Q^\alpha Q^\beta}{Q^2}\right)\mathcal{S}^{\alpha\beta}(\vec{Q},\omega)\ . \tag{6}$$

Here α,β denote Cartesian components. The scattering function $\mathcal{S}^{\alpha\beta}(\vec{Q},\omega)$ is related to the wavevector-dependent susceptibility $\chi^{\alpha\beta}(\vec{Q})$ and the normalized spectral shape function $F^{\alpha\beta}(\vec{Q},\omega)$ through

$$\mathcal{S}^{\alpha\beta}(\vec{Q},\omega)=\frac{\chi^{\alpha\beta}(\vec{Q})}{\chi^0}\frac{\hbar\omega\beta}{1-e^{-\hbar\omega\beta}}F^{\alpha\beta}(Q,\omega)\ , \tag{7}$$

with

$$\int_{-\infty}^{\infty}F^{\alpha\beta}(\vec{Q},\omega)\,d\omega=1\ \text{ for any }\vec{Q}\ . \tag{8}$$

Here χ^0 represents the susceptibility of noninteracting magnetic moments. The two-dimensional character of the correlations implies that $\chi^{\alpha\beta}(\vec{Q})$ does not depend on Q_z. The critical scattering thus forms ridges parallel to the c^* axis at $h=1$, 3, etc., as indicated by the cross hatching in the left-hand part of Fig. 1. The width across the ridge gives the inverse correlation range in the sheets.

When $\hbar\omega\beta=\hbar\omega/k_BT\ll 1$, the second factor in Eq. (7) varies linearly with ω, so with the normalization condition as expressed in Eq. (8) we find that

$$\mathcal{S}^{\alpha\beta}(\vec{Q},\omega)\,d\omega\simeq\frac{\chi^{\alpha\beta}(\vec{Q})}{\chi^0}=\langle S^\alpha_{-\vec{Q}}(0)S^\beta_{\vec{Q}}(0)\rangle_T\ . \tag{9}$$

Utilizing the fact that $\chi^{\alpha\beta}(\vec{Q})$ is independent of Q_z, the integration is carried out quite accurately by the instrument if $\vec{k}_f$ is parallel to the c axis. This point is discussed in detail in Ref. 7. Finally, we comment on the summation over α, β in Eq. (6). The weight factor $(\delta_{\alpha\beta}-Q_\alpha Q_\beta/Q^2)$ arises basically from the geometry of the dipolar interaction between the magnetic moments of the ions and of the neutrons in an unpolarized neutron beam. For systems with Heisenberg interactions and uniaxial anisotropy only the diagonal components $\alpha=\beta$ are nonvanishing in $\chi^{\alpha\beta}$, so we find

$$\sigma(\vec{k}_i\to\vec{k}_f)=[1+(Q_z/Q)^2]\mathcal{S}^\perp(\vec{Q},\omega)+[1-(Q_z/Q)^2]\mathcal{S}^\parallel(\vec{Q},\omega)\ , \tag{10}$$

where the superscripts $\perp$ and $\parallel$ indicate transverse and longitudinal response functions, respectively.

B. Experimental configuration

The measurements on K_2NiF_4 and the random alloy $Rb_2Mn_{0.5}Ni_{0.5}F_4$ were carried out at the Brookhaven High Flux Beam Reactor whereas the measurements on K_2MnF_4 were carried out at the cold source facility in the DR3 reactor at Risø. The experimental configurations were quite similar. Monochromatic neutrons were extracted from the reactor beam by Bragg reflection from a curved pyrolytic graphite monochromator using the (0 0 2) reflection. The *direction* of $\vec{k}_f$ was determined by a collimator in front of the detector but in order to carry out the integration over ω by the instrument no energy analyzer was applied. The finite collimation and mosaic spreads of the monochromator and of the sample give rise to an instrumental Q resolution, but as $\chi(\vec{Q})$ is independent of Q_z it is only the resolution width δ_x across the ridge and the vertical resolution width δ_y that affect the measured intensity. The Q resolution was measured by the line profile of Bragg scattering and the widths δ_x and δ_y agreed with calculated widths typically within 5%.

C. Qualitative description of $\chi^\parallel(Q)$ and $\chi^\perp(Q)$

Figure 4 shows scans across the $h=1$ ridge for K_2NiF_4 at 90 K and at 97.334 K ($T_N=97.23$ K). The incident wave vector of 2.5 Å^{-1} implies that $\vec{k}_f$ is parallel to the c axis when the *elastic* scattering

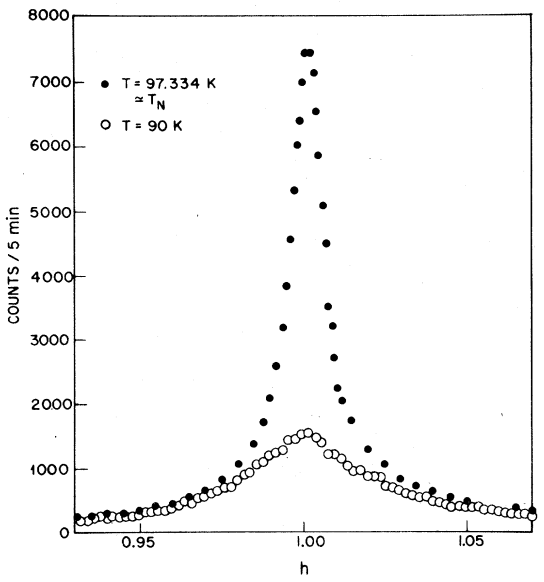

FIG. 4. Scans across the ridge at the value of l where the quasielastic approximation is nearly exact. The 90-K data are dominated by $\chi^{\perp}$ whereas the data close to T_N represent the sum of $\chi^{\perp}+\chi^{\parallel}$.

process corresponds to the Q_z component of $\sim 0.5c^*$. In that case the cross section of Eq. (10) gives the transverse and the longitudinal response with about equal weights. As the temperature is decreased below T_N, $\chi^{\parallel}$ disappears rapidly [cf. $\chi^{\parallel}(q=0,-\Delta T)=\frac{1}{57}\chi^{\parallel}(q=0,+\Delta T)$ for the 2D Ising model].[4] The scan at 90 K, that is 7% below T_N, thus is dominated by the transverse susceptibility $\chi^{\perp}(\vec{q})$. We may interpret $\chi^{\perp}(\vec{q})$ quantitatively by considering the spin-wave cross section for $T<T_N$. For energies $\hbar\omega/kT \ll 1$ the population factor in the spin-wave cross section is proportional to $(\hbar\omega)^{-1}$, and as the dynamical structure factor is also inversely proportional to $(\hbar\omega)^{-1}$[cf. Eq. (7) of Ref. 15] one finds for the spin-wave intensity at wave vector $(q_x,0,0)$

$$I_{SW}(q_x) \propto (\hbar\omega)^{-2} \propto [(\pi q_x)^2 + 2h_A + h_A^2]^{-1} , \qquad (11)$$

with the reduced anisotropy field h_A as given in Table I. Here $\vec{q}=\vec{\tau}-\vec{Q}$, where $\vec{\tau}$ is a magnetic reciprocal-lattice vector. Since $h_A \ll 1$ the transverse half width $\kappa^{\perp}$ in units of a^* is given by $\pi\kappa^{\perp}$ $=(2h_A)^{1/2}$. This treatment assumes classical spins; a more accurate formula is[9]

$$(\pi\kappa^{\perp}) = [2h_A/(1-R_0)]^{1/2} , \qquad (12)$$

with the correction term R_0 being -0.08 for Ni and -0.032 for Mn. For K_2NiF_4, Eq. (12) gives $\kappa^{\perp}=0.02a^*$ in excellent agreement with the half width of the 90 K scan in Fig. 4. In each of K_2NiF_4, K_2MnF_4, and $Rb_2Mn_{0.5}Ni_{0.5}F_4$ we, in fact, find that $\kappa^{\perp}$ is independent of temperature for $T<0.95T_N$ provided, of course, that the condition $\hbar\omega/kT \ll 1$ is satisfied for the long-wavelength spin waves. The values so obtained for $\kappa^{\perp}$ together with corresponding spin-wave values are given in Table III. In general the agreement is quite good for all three compounds although the experimental $\kappa^{\perp}$ is consistently about 15% lower than $\kappa^{\perp}$ (spin wave). This effect originates from the wave-vector dependence of the spin-wave renormalization with temperature. We should emphasize that the dominance of spin-wave scattering in the measured $\chi^{\parallel}(Q)+\chi^{\perp}(Q)$ for $T<0.95\ T_N$ has previously been noted by Birgeneau *et al.*[7] in their dynamics measurements in K_2NiF_4 and by Ikeda and Hirakawa[8] in their quasielastic measurements in K_2MnF_4. The above simply puts that observation on a quantitative basis.

TABLE III. Transverse correlation length below T_N.

Compound	$\kappa^{\perp}$ (measured) units of a^*	$\kappa^{\perp}$ (spin wave) units of a^*
K_2NiF_4	0.017	0.0195
K_2MnF_4	0.024	0.27
$Rb_2Mn_{0.5}Ni_{0.5}F_4$	0.035	0.040

As the temperature is raised towards T_N the longitudinal susceptibility diverges[7,8] whereas the transverse susceptibility is approximately constant up to T_N. Thus the differences in the intensities between 97.334 and 90 K evident in Fig. 4 represents mainly $\chi^{\parallel}(\vec{q})$ at T_N. The fact that the intensity at $h=1$ has not actually diverged is due to the finite q resolution. Figure 5 shows the temperature dependence of the width and of the peak intensity of data similar to those in Fig. 4. In the top part, the level around 140 represents the temperature-independent transverse staggered susceptibility for $T/T_N<1$. In Sec. IV D we shall discuss the assessment of $\chi^{\perp}$ above T_N; here it suffices to note the transverse susceptibility constitutes a significant part of the total intensity and it must be corrected for before one can deduce critical exponents, etc., of the diverging longitudinal susceptibility. From the bottom part of Fig. 5 we conclude as discussed above that the resulting full width at half maximum is determined by spin-wave scattering up to $T/T_N \simeq 0.95$, whereas the longitudinal response dominates in the region $0.99 < (T/T_N) < 1.05$. Quite similar results were also found in K_2MnF4 and in the random alloy $Rb_2Mn_{0.5}Ni_{0.5}F_4$.

It is important to emphasize that this picture of the data only emerges if the instrument is set for proper integration over ω, that is, with $\vec{k}_f$ along the c axis. As an illustration we show in Fig. 6

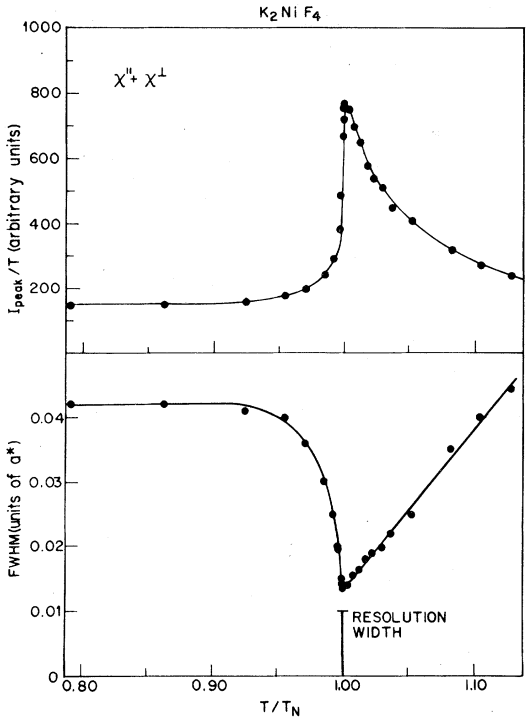

FIG. 5. Peak intensity divided by temperature and full width at half maximum across the $h=1$ ridge vs temperature. With ideal q resolution the upper curve would represent $0.95\chi'' + 1.05\,\chi^{\perp}$.

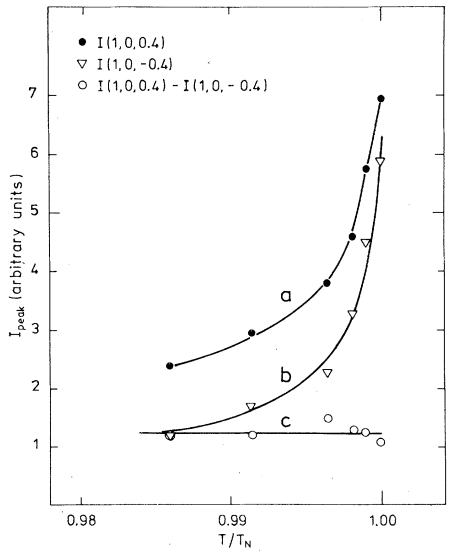

FIG. 6. Peak intensity below T_N at $l=0.4$, where the quasielastic approximation is nearly exact (curve a) and at the symmetric point $l=-0.4$ (curve b) where the quasielastic approximation fails severely for the strongly inelastic transverse fluctuations. The difference between a and b (curve c) represents primarily the transverse susceptibility.

data taken with momentum transfer $\vec{Q}$ for elastic scattering set at (1,0,0.4) and (1,0,−0.4) in K_2NiF_4. In the former case $\vec{k}_f$ is parallel to c^* so these data are analogous to those in the top part of Fig. 4. With $\vec{Q}=(1,0,-0.4)$ the constant $-Q_z$ condition for inelastic scattering processes is far from being fulfilled and as the transverse spin-wave scattering is much more inelastic than the longitudinal critical scattering (cf. Figs. 4 and 5 in Ref. 7), the transverse spin-wave scattering hardly contributes to the total scattering in that case. The difference between the intensities at (1,0,0.4) and (1,0,−0.4) thus represents mainly $\chi^{\perp}$. The staggered transverse susceptibility appears to be independent of temperature right up to T_N and one cannot, within the experimental accuracy, even detect a mild cusp at T_N as was seen in MnF_2 by Schulhof *et al.*[19] Similar results for $\chi^{\perp}$ have been obtained by Binder and Landau[13] in their computer experiments. A general survey of the q dependence of the scattering at 77 K in K_2NiF_4 shows that the integration over energy[7] of the spin waves is only properly performed for $0 \leq l \leq 1$. Otherwise the scattering appears to be very weak and Q independent. Thus the scans at (1, 0, 6.8) in Ref. 7 provide no information whatsoever about $\chi^{\perp}(\vec{Q})$.

The final feature in our qualitative discussion of the two-axis data is shown in Fig. 7. The scan across the $h=1$ ridge at $T/T_N=0.74$ in the random system exhibits a narrow, resolution-limited

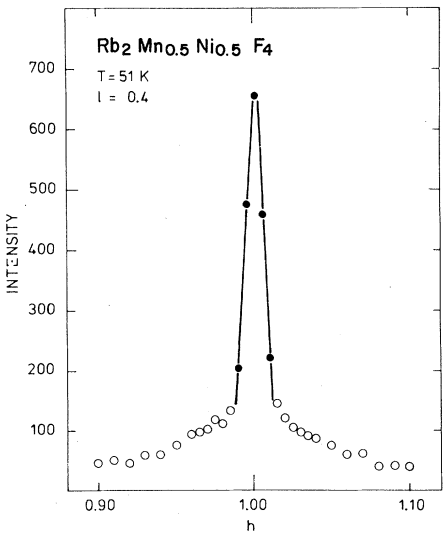

FIG. 7. Scan across the ridge at $T/T_N=0.74$ in the site-random alloy. The narrow peak at $h=1$ (full circles) is presumably due to regions in the crystal between the domains where the ordering is only two dimensional. Data at $T<T_N$ with $0.99<h<1.01$ were discarded from the analysis.

peak at $h=1$ superimposed on the broader transverse susceptibility peak. The latter decreases with decreasing temperature, since the cross section is proportional to $T\chi$ whereas the narrow line increases with decreasing temperature, qualitatively like the squared order parameter. Fortunately it is easy to separate the two components of the scattering due to their different widths and temperature dependence. Tentatively we may interpret this narrow line in the random crystal as being due to two-dimensional magnetic Bragg scattering from regions in the crystal where the spins cannot decide whether to form the three-dimensional K_2NiF_4 structure or the Ca_2MnO_4 structure. This interpretation is consistent with the fact that the narrow line is much more pronounced in the random system where both these phases coexist as ordered phases. In the pure materials the narrow line is at least an order of magnitude smaller and therefore not visible in the two-axis data but it is clearly visible in three-axis data of ω scans at constant Q as a narrow peak around $\omega=0$ (see Fig. 4 of Ref. 7). In that case an alternate explanation in terms of the difference between χ_T and χ_S has been offered.

D. Analysis and results

In this section we shall describe our method of analysis for the divergent longitudinal susceptibility $\chi^{\parallel}(q=0,t)$ and the inverse correlation range $\kappa^{\parallel}(t)$ in the three materials. Tracy and McCoy[12] have shown that for the 2D Ising model for $T>T_N$ the Lorentzian approximation $\chi^{\parallel}(q)\propto(q^2+\kappa^2)^{-1}$ is very accurate for $q<10\kappa$. In order to keep the analysis of our results at a reasonably simple level we have discarded data with $q>10\kappa$, and we have assumed a cross section $\sigma(q)$ of the form

$$\sigma(\vec{q})=T[A^{\parallel}/(q_x^2+q_y^2+\kappa^{\parallel 2})+A^{\perp}/(q_x^2+q_y^2+\kappa^{\perp 2})]\ . \quad (13)$$

The observed intensities are then fitted in a least-squares sense to the cross section folded with the instrumental resolution function

$$R(q_x,q_y)=\exp(-q_x^2/\delta_x^2-q_y^2/\delta_y^2)\ . \quad (14)$$

The resolution parameters δ_x and δ_y were determined experimentally from the $(1,0,0)$ Bragg scattering line profiles.

As discussed in the previous subsection for $T\lesssim 0.95T_N$, $\sigma(\vec{q})$ is dominated by $\chi^{\perp}(\vec{q})$ and one finds $A^{\perp}$ and $\kappa^{\perp}$ to be independent of temperature. This corresponds exactly to what one expects on the basis of the mean-field approximation for $\chi^{\perp}$. It is also evident from Figs. 4 and 6 that this behavior for $\chi^{\perp}$ persists right up to T_N. As noted above, similar results are obtained by Binder and Landau[13] who find firstly that there is no cusp evident in $\chi^{\perp}$ at T_N and secondly $\chi^{\perp}(T_N)$ agrees rather well with the theoretical value based on spin-wave theory. Least-squares fits of the critical scattering data in the immediate vicinity of T_N to Eq. (13) with $A^{\perp}$ and $\kappa^{\perp}$ fixed at their $T\leq T_N$ values then yields best fit values for $A^{\parallel}$ and $\kappa^{\parallel}$. Satisfactory fits are obtained in all three systems with goodness of fit parameters. $\chi^2\sim 1$, thus showing the adequacy of Eq. (13) to represent the data. It is of interest to compare this with the original analysis given in Ref. 7 of the K_2NiF_4 data near T_N. In this approach those authors essentially omitted $\chi^{\perp}$ based on their misleading results at $\vec{Q}=(1,0,6.8)$. Not surprisingly, they then found that a single Lorentzian was completely inadequate near T_N. However, improved fits could be obtained by using a Fisher-Burford approximant $\sigma(\vec{q})\sim(\kappa^2+q^2)^{-1+\eta/2}$, with η temperature dependent. This yielded $\eta(T_N)\simeq 0.4$; however the fits were still rather poor with $\chi^2\sim 4$. It is now clear that this method of data analysis is simply incorrect and that Eq. (13) with the predetermined values for $A^{\perp}$ and $\kappa^{\perp}$ gives the proper functional form for $\sigma(\vec{q})$ in the immediate vicinity of T_N.

We now consider the analysis of the data further above T_N. As noted above, the data at T_N are clearly the sum of a narrow and a broad Lorentzian. Further above T_N however such a simple visual separation is no longer possible. In the absence of separate measurements of $\chi^{\parallel}$ and $\chi^{\perp}$ then several options are open. The most physically plausible approach is to assume a generalized mean field behavior for $\chi^{\perp}$; that is, $A^{\perp}$ is fixed at its value at T_N while $\kappa^{\perp}$ is assumed to follow the same power law as $\kappa^{\parallel}$ but with a shifted T_N. The shift in T_N is fixed by the requirement that $\kappa^{\perp}(T>T_N)$ achieve the spin-wave value at T_N. It turns out empirically that $\Delta T^{\perp}/T_N\simeq 0.2$ in all three systems. At the other extreme, one may assume that $A^{\perp}$ and $\kappa^{\perp}$ are temperature independent within the critical region. Fortunately the final results for the critical exponents γ, ν in all three systems are independent of the detailed assumptions about $A^{\perp}$, $\kappa^{\perp}$ to within the errors. The only essential feature is that $\chi^{\perp}(\vec{q})$ be included properly at T_N. Because of this insensitivity to the detailed approximations we present only the results for the data analyzed with the generalized mean-field approximation.

The relative magnitudes of $\chi^{\parallel}(q=0,t)$ and $\chi^{\perp}(q=0,t)$ for K_2NiF_4 are given in Fig. 8. It should be noted that the vertical scale is logarithmic. The corresponding results on a linear scale for $Rb_2Mn_{0.5}Ni_{0.5}F_4$ are shown in Fig. 9. Similar results are obtained in K_2MnF_4.

In Fig. 10 we show $\kappa^{\parallel}$ versus temperature over

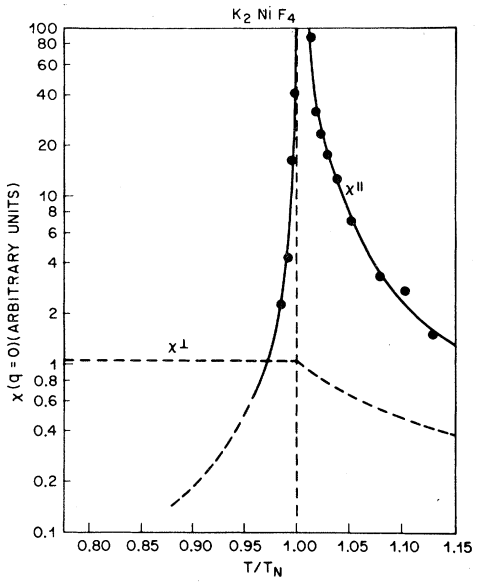

FIG. 8. Transverse and longitudinal staggered susceptibility in K_2NiF_4. Note the logarithmic scale on the ordinate.

a wide temperature range in $Rb_2Mn_{0.5}Ni_{0.5}F_4$. The estimated values for $\kappa^{\perp}$ above T_N are shown by the dotted line. The open circles above T_N give the values for $\kappa^{\parallel}$ deduced using $\kappa^{\perp}$ fixed at these values. Note that only the point at 80 K is appreciably changed if one takes instead $\kappa^{\perp} = \text{const} = 0.035a^*$. The two points at 100 and 117 K are obtained from fits to a single Lorentzian, that is, by assuming $\chi^{\parallel}(\vec{q}) = \chi^{\perp}(\vec{q})$. Not surprisingly, they lie on a smooth extrapolation of the data for T near

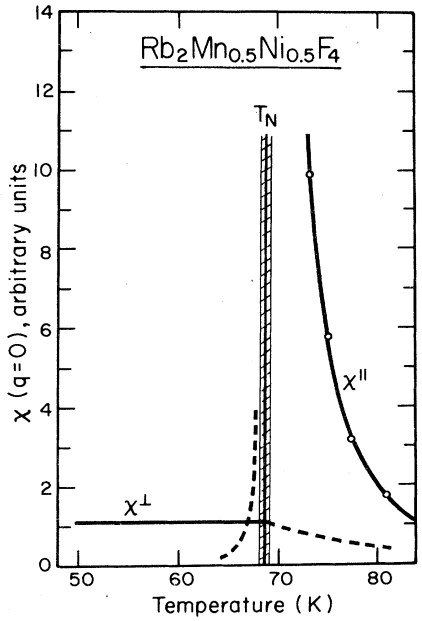

FIG. 9. Least-squares-fitted values for $\chi^{\parallel}(0)$ and $\chi^{\perp}(0)$ above and below T_N in $Rb_2Mn_{0.5}Ni_{0.5}F_4$. The cross-hatched area represents the region of smearing of T_N. The dashed lines are schematic representations of the behavior of $\chi^{\parallel}$ below and $\chi^{\perp}$ above T_N.

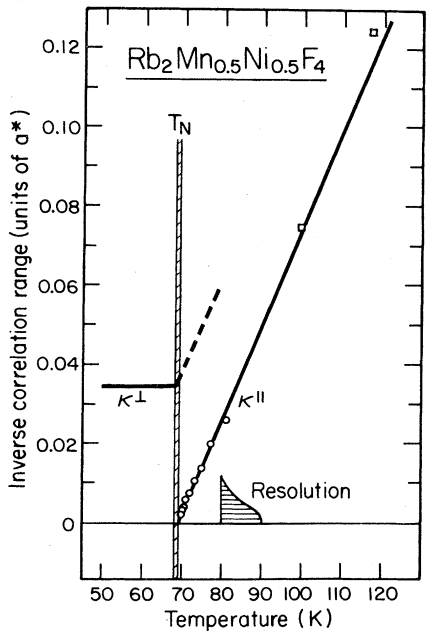

FIG. 10. Best-fit values for $\kappa^{\parallel}$ and $\kappa^{\perp}$ in $Rb_2Mn_{0.5}Ni_{0.5}F_4$. The meaning of T_N is indicated by the cross-hatched column. The instrumental distribution of wave vectors is indicated by the curve marked resolution.

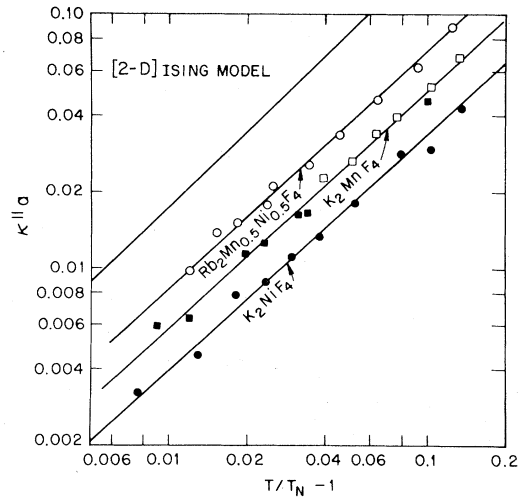

FIG. 11. Double-log plot of the inverse correlation range κ times the nearest-neighbor distance a vs the reduced temperature variable $(T - T_N)/T_N$ for the pure materials K_2NiF_4 (●), K_2MnF_4 (□,■), and the site-random alloy $Rb_2Mn_{0.5}Ni_{0.5}F_4$(○). The theoretical curve for the two-dimensional Ising model is also shown.

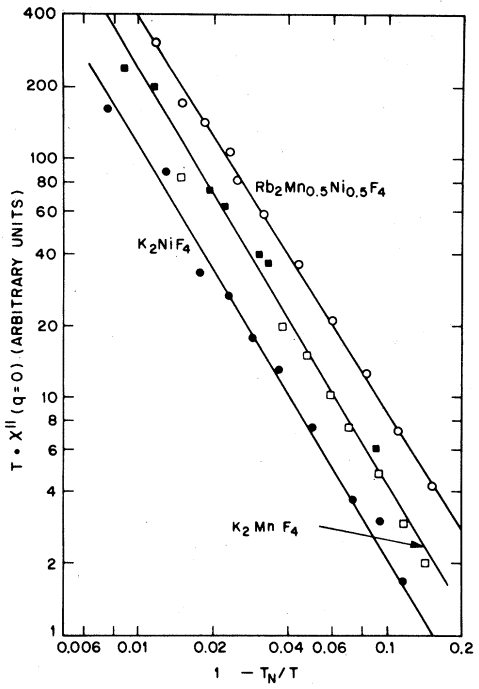

FIG. 12. Double-log plot of the staggered susceptibility $\chi(q=0,t)/\chi^0$ vs the reduced temperature $(T-T_N)/T$ for K_2NiF_4 (●), K_2MnF_4 (□,■), and $Rb_2Mn_{0.5}Ni_{0.5}F_4$(○). Note that each curve is given in different arbitrary units.

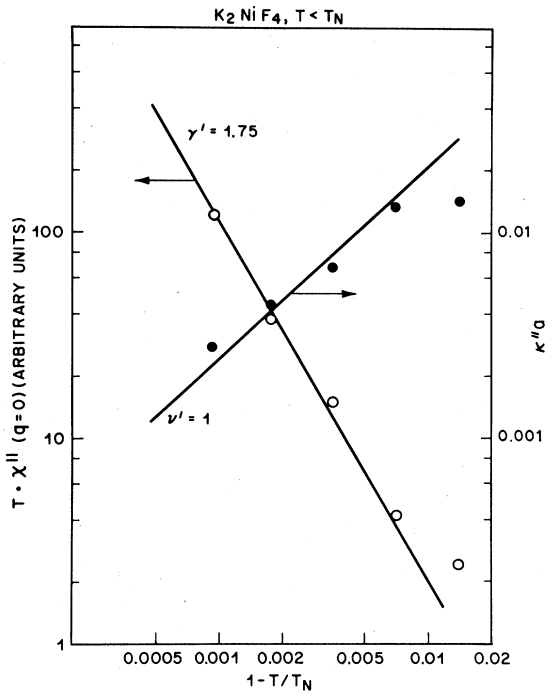

FIG. 14. Data for $\chi^{II}(q=0)/\chi^0$ and κ^{II} below T_N in K_2NiF_4.

T_N. From Fig. 10 it is also evident that resolution effects are crucial near T_N.

The final results for $T > T_N$ are summarized in Figs. 11–13. Figure 11 shows κ^{II} vs $T/T_N - 1$. In order to compare the data in dimensionless units κ^{II} is multiplied by the nearest-neighbor distance a. The results are fitted to power laws of the form

$$a\kappa^{II} = F(T/T_N - 1)^{\nu} \tag{15}$$

and the results for F and ν are given in Table II.

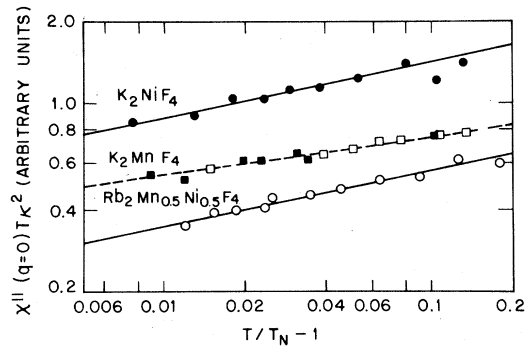

FIG. 13. Double-log plot of $\chi^{II}(q=0)\kappa^2 T \propto \kappa^{\eta}$ vs reduced temperature $(T-T_n)/T_N$. The slope is the produce of the exponents ν and η.

All three materials exhibit the same critical behavior with 2D Ising-like exponents and with the magnitude of the correlation range at a given temperature tending towards the Ising value as the anisotropy field h_A [cf. Eq. (2)] increases.

Figure 12 shows the staggered susceptibility $\chi^{II}(q=0)/\chi^0 \propto TA^{II}/\kappa^{II2}$ versus the reduced temperature $(T-T_N)/T$ in arbitrary units. Again the results are fitted to power laws of the form

$$\chi(q=0)/\chi^0 = C(1 - T_N/T)^{-\gamma}\ , \tag{16}$$

with the values of γ given in Table II.

Figure 13 shows $\kappa^{II2}\chi(q=0)/\chi^0 = A^{II}(T/T_N)$ vs $(T/T_N - 1)$. Since $\chi^{II}(q)/\chi^0 \propto \kappa^{II\eta}/(\kappa^{II2} + q^2)$ the quantity $(T/T_N)A^{II}$ is proportional to κ^{η}, i.e.,

$$(T/T_N)A^{II} \propto (T/T_N - 1)^{\eta\nu}. \tag{17}$$

The least-squares-fitted values of the power $\eta\nu$ are given in Table II.

Finally we show in Fig. 14 our data for $\chi^{II}(q=0)/\chi^0$ and $a\kappa^{II}$ below T_N for K_2NiF_4. The unfolding of the instrumental resolution effect necessitates a known form of the cross section. We used the Lorentzian cross section for Eq. (13), but this form may be quite inaccurate below T_N as pointed out by Tarko and Fisher.[20] On the other hand, our data are not detailed enough to be fitted to a more sophisticated expression for $\chi^{II}(q)$. Our results for $\chi^{II}(q=0)/\chi^0$ and $a\kappa^{II}$ below T_N may therefore be

subject to considerable systematic errors and a least-squares fit to power laws is not in order. We do indicate though that our data are consistent with 2D Ising values $\gamma' = 1.75, \nu' = 1$. Furthermore the ratio of $\chi''(q=0,-\Delta T)/\chi''(q=0,+\Delta T)$ is $\sim 50 \pm 10$, to be compared with the value of 37 for the 2D Ising model. The smearing of T_N makes it impossible to obtain similar data in the random alloy.

V. DISCUSSION AND CONCLUSIONS

We discuss first the general results and their significance for our overall understanding of these 2D systems. We shall then consider the aspects special to the random magnet problem. As noted above the principal results of these experiments are contained in Figs. 11–13. As originally expected, near T_N, the pathology associated with the 2D Heisenberg Hamiltonian is lifted by the anisotropy terms and a 2D Ising transition is observed. It has been known for some time that only $\chi''(0)$ diverges; we now find in addition that all exponents are at least close to those of the idealized 2D Ising model. The reduced temperature range covered is from ~0.15 to ~0.008; the corresponding range in correlation length is from ~20 to 250 lattice units. The limiting value of $250a$ is determined by the instrumental resolution (cf. Fig. 10) and not by temperature control or any smearing of T_N. These experiments thus probe as close to the critical point as previous neutron scattering measurements in other systems. It seems most likely that the difference between the experimentally determined exponents and those of the 2D Ising model is due to the fact that we simply are not yet in the asymptotic regions. We should reemphasize that the scattering geometry itself shows explicitly that the correlations are (a) purely two-dimensional; (b) Ising-like—hence the above conclusions.

The data for $\chi''(0)$ have not been put on an absolute scale so we can make no relative comparisons between the three systems studied. For K_2NiF_4 there is an enormous asymmetry in $\chi''(0)$ about T_N, that is, $\chi''(-|\epsilon|) \approx 0.02\chi''(|\epsilon|)$. This is in agreement with one's expectations based on the 2D Ising model. The correlation length data can, however, be put on an absolute scale and indeed, as shown in Fig. 11, there is a very interesting trend. As h_a increases from ~0.002 to ~0.007, $\kappa'' a$ moves rapidly towards the 2D Ising value ($h_a = 1$). There is currently no theory for such an effect.

In a previous paper we have reported a study of the spin correlations in $Rb_2Mn_{0.5}Ni_{0.5}F_4$ in the precritical region, that is for $1.1 < T/T_N < 2$. Over that temperature range the measured combination $0.95\chi''(\vec{q}) + 1.05\chi^{\perp}(\vec{q})$ could be adequately described by a single Lorentzian. These measurements then yield directionally averaged values for $\chi(0)$ and κ. Perhaps coincidentally, these averaged values can be described by power laws with 2D Ising exponents $\gamma \sim = 0.75$, $\nu \sim 1$. There is some evidence for a crossover to a 2D Heisenberg value ($\gamma \sim 2.3$) for $T > 1.5$ T_N. If, as seems most likely, these results apply to the pure systems as well, then they offer an immediate explanation of the electron-spin-resonance (ESR) results of de Wijn *et al.*[21] These authors find that in the precritical region, $1.1 < T/T_N < 2$, the EPR linewidth in K_2MnF_4 diverges like $(T/T_N - 1)^{-2.5\pm0.2}$. Simple random-phase theory which is only applicable to the precritical region (see the papers listed in Ref. 22 for a detailed discussion of the appropriate approximations) predicts $\Delta H \sim (T/T_N - 1)^{-2\gamma+\nu(d-z)}$, where the dynamical scaling index $z = 1$ in $d = 2$ dimensions. From the results of Ref. 15 we have $-2\gamma + \nu = -2.5$ in exact agreement with experiment. Bucci and Guidi[23] have shown that similar agreement is obtained for the nuclear-magnetic-resonance linewidth in K_2MnF_4 in the precritical region.

Finally in this general discussion we should also like to consider briefly some recent experiments in $K_2Mn_{1-x}Fe_xF_4$. The anisotropy for Mn^{++} is Ising-like whereas that for Fe^{++} is XY-like. There will also be a small cubic anisotropy. In a very interesting neutron scattering experiment, Bevaarts *et al.*[24] show that in two samples with $x \sim 0.023$ and $x \sim 0.028$ the mean anisotropy h_A is very near zero. Their quasielastic neutron scattering experiments then yield ridge intensities very much like those shown in Fig. 5 for K_2NiF_4 except that the ridge intensity below T_N is some what enhanced. Further, the ridge width appears to be quite small. They have attributed this 2D scattering for $T < 0.95$ T_N to regions in the crystal with 2D long-range order. It seems clear, however, from our discussion in Sec. IV C that they are simply observing the spin-wave scattering in a system with small h_A and hence a small $\kappa^{\perp}$—no more exotic explanation is required. For $x = 0.023$ the spins point along [001] near T_N while for $x = 0.028$ the spins are aligned along [110]. In both samples there is a spin-reorientation transition at lower temperatures. Bevaarts *et al.*[24] have suggested that this lower transition corresponds to a gradual increase in the 3D long-range order. We should like to offer an alternate and, we think, more convincing explanation. A consideration of the spin Hamiltonian for these mixed crystals suggests instead that $K_2Mn_{1-x}Fe_xF_4$ is exhibiting *tetracritical* behavior of the sort discussed by Bruce and Aharony[25] for a system with competing second- and fourth-order anisotropies. Indeed, the correspondence between

the results of Bevaarts *et al.*[24] and the theoretical phase diagram (their Fig. 3) of Bruce and Aharony is remarkable. Clearly further work on this most interesting system would be of considerable value.

We conclude this paper with a brief discussion on the effects of randomness on critical behavior. As first predicted by Harris[11] on the basis of a heuristic argument, site or bond randomness should be irrelevant for systems with a specific-heat exponent $\alpha<0$. For $\alpha>0$ randomness should be a "relevant" variable and indeed recent renormalization group (RG) calculations[11] indicate that such systems will exhibit a sharp phase transition with subtly renormalized exponents. For $\alpha=0$ one anticipates a sharp phase transition with pure system exponents modified by logarithmic corrections.[26] Given the subtle effects for $\alpha>0$ these logarithmic corrections may be unobservable in any real experiment.

The experiments reported here give strong support to the above predictions. The transition in $Rb_2Mn_{0.5}Ni_{0.5}F_4$ is, of course, not perfectly sharp. However, the observed rounding appears to correlate strongly with the macroscopic size of the sample and, by inference, to macroscopic chemical gradients. In any case, the critical scattering experiments show that above T_N the correlated clusters contain >40 000 spins before the smeared region is entered. The exponents in $Rb_2Mn_{0.5}Ni_{0.5}F_4$ are identical to those in the pure systems K_2NiF_4 and K_2MnF_4. Further, all three systems correspond closely to the 2D Ising model for which, of course, $\alpha=0$. We conclude therefore that, as anticipated, any logarithmic corrections to the randomness are unobservably small in our experiments.

Equation of state measurements[27] have been reported in the amorphous metallic ferromagnets $Co_{0.7}B_{0.2}P_{0.1}$ and $Fe_{0.8}P_{0.13}C_{0.07}$. These systems most likely fall in the universality class $d=3, n=3$ for which $\alpha<0$. In both cases sharp phase transitions are observed with exponents similar to those in the crystalline transition metals Fe and Ni. Again these results are consistent with current theory. Amorphous transition-metal alloys, that is systems which combine site randomness with bond randomness, however, seem to exhibit severly broadened transitions.[27] These results are difficult to understand within the existing framework although the broadening could simply reflect difficulties in the metallurgy rather than shortcomings in the theory. Finally, Pickart *et al.*[28] in their study of amorphous $TbFe_2$ find that the correlation length appears to be finite at T_c. However, this system combines randomness in the exchange interaction with a randomly oriented crystal field. This is a rather more complicated model in which disorder may effect the critical behavior in an especially complicated fashion. RG calculations by Aharony[11] for the above system provide a possible explanation although additional theory and experiments are probably still required.

It is clear that further work remains to be done on the random magnet problem. Nevertheless we believe that with the completion of this work the 2D near-Heisenberg magnets typified by K_2NiF_4 both pure and site random, are now well understood.

ACKNOWLEDGMENTS

We should like to thank John Skalyo, Jr., for his participation in the early stages of this experiment and for his advice on the data analysis. We should also like to thank A. Aharony, B. I. Halperin, K. A. Binder, D. P. Landau, T. C. Lubensky, and D. R. Nelson for interesting and helpful conversations.

---

*Present address; work at M. I. T. supported by the NSF.

†Work at Brookhaven performed under the auspices of the USERDA.

[1]For a review of work up until 1974 see L. J. de Jongh and A. R. Medema, Adv. Phys. 23, 1 (1974); for more recent work see G. Shirane and R. J. Birgeneau, Physica B (Utr.) 86–88, 639 (1977).

[2]R. J. Birgeneau, H. J. Guggenheim, and G. Shirane, Phys. Rev. Lett. 22, 720 (1969); Phys. Rev. B 1, 2211 (1970); 8, 304 (1973).

[3]H. Ikeda and H. Hirakawa, Solid State Commun. 14, 529 (1974); E. J. Samuelson, J. Phys. Chem. Solids 35, 785 (1973).

[4]L. Onsager, Phys. Rev. 5, 117 (1944); C. N. Yang, *ibid.* 85, 809 (1952); B. M. McCoy and T. T. Wu, *The Two-Dimensional Ising Model* (Harvard University, Cambridge, Mass. 1973).

[5]H. E. Stanley and T. R. Kaplan, Phys. Rev. Lett. 17, 913 (1966); J. M. Kosterlitz and D. J. Thouless, J. Phys. C 5, L124 (1972); 6, 1181 (1973); R. A. Pelcovits and D. R. Nelson, Phys. Lett. A 57, 23 (1976).

[6]R. J. Birgeneau, J. Skalyo, Jr., and G. Shirane, J. Appl. Phys. 11, 1303 (1970).

[7]R. J. Birgeneau, J. Skalyo, Jr., and G. Shirane, Phys. Rev. B 3, 1736 (1971).

[8]H. Ikeda and K. Hirakawa, J. Phys. Soc. Jpn. 33, 393 (1972); 35, 617 (1973).

[9]H. W. de Wijn, L. R. Walker, and R. E. Walstedt, Phys. Rev. B 8, 285 (1973).

[10]E. K. Riedel and F. J. Wegner, Z. Phys. 225, 195 (1969).

[11]A. B. Harris, J. Phys. C 7, 1671 (1974); A. B. Harris and T. C. Lubensky, Phys. Rev. Lett. 33, 1540 (1974); T. C. Lubensky, Phys. Rev. B 11, 3580 (1975); V. Emery, *ibid.* 11, 239 (1974); A. Aharony, *ibid.* 12, 1038 (1975); G. Grinstein and A. Luther, *ibid.* 13, 1329 (1976); D. E. Khmel'nitsky, Zh. Eksp. Teor. Fiz. 68, 1960 (1975).

[12]C. A. Tracy and B. M. McCoy, Phys. Rev. Lett. 31, 1500 (1973); Phys. Rev. B 12, 368 (1975); C. A. Tracy, AIP Conf. Proc. 29, 483 (1976).

[13]K. Binder and D. P. Landau, Phys. Rev. B 13, 1140 (1976).

[14]J. Als-Nielsen, R. J. Birgeneau, H. J. Guggenheim, and G. Shirane, J. Phys. C 9, L121 (1976).

[15]J. Als-Nielsen, R. J. Birgeneau, H. J. Guggenheim, and G. Shirane, Phys. Rev. B 12, 4963 (1975).

[16]D. E. Cox, G. Shirane, R. J. Birgeneau, and J. B. MacChesney, Phys. Rev. 188, 930 (1969).

[17]M. E. Lines, Phys. Rev. 164, 736 (1967).

[18]For a general discussion of neutron scattering see W. Marshall and S. W. Lovesey, *Theory of Thermal Neutron Scattering* (Oxford University, New York, 1971).

[19]M. P. Schulhof, R. Nathans, P. Heller, and A. Linz, Phys. Rev. B 4, 2254 (1971).

[20]H. B. Tarko and M. E. Fisher, Phys. Rev. B 11, 1217 (1975).

[21]H. J. de Wijn, L. R. Walker, J. L. Davis, and H. J. Guggenheim, Solid State Commun. 11, 803 (1972).

[22]K. Kawasaki, Prog. Theor. Phys. 39, 285 (1968); D. L. Huber, J. Phys. Chem. Solids 32, 2145 (1971); and Phys. Rev. B 6, 3180 (1972); R. J. Birgeneau, L. W. Rupp, Jr., H. J. Guggenheim, P. A. Lindgard, and D. L. Huber, Phys. Rev. Lett. 30, 1252 (1973).

[23]C. Bucci and G. Guidi, Phys. Rev. B 9, 3053 (1974).

[24]L. Bevaart, J. V. Lebesque, E. Frikee, and L. J. de Jongh (unpublished).

[25]A. D. Bruce and A. Aharony, Phys. Rev. B 11, 478 (1975). We thank D. Nelson for drawing our attention to this paper and for a most helpful discussion.

[26]M. Suzuki, J. Phys. C 8, 255 (1975); U. Krey, Physica (Utr.) B 83, 349 (1976).

[27]T. Mizoguchi, N. Ueda, K. Yawauchi, and H. Miyajima, J. Phys. Soc. Jpn. 34, 1691 (1973); K. Yamoda, Y. Ishikawa, Y. Endoh, and T. Masumoto, Solid State Commun. 16, 1335 (1975).

[28]S. J. Pickart, J. J. Rhyne, and H. A. Alperin, Phys. Rev. Lett. 33, 424 (1974).